Acute histopathological responses and long-term behavioral outcomes in mice with graded controlled cortical impact injury
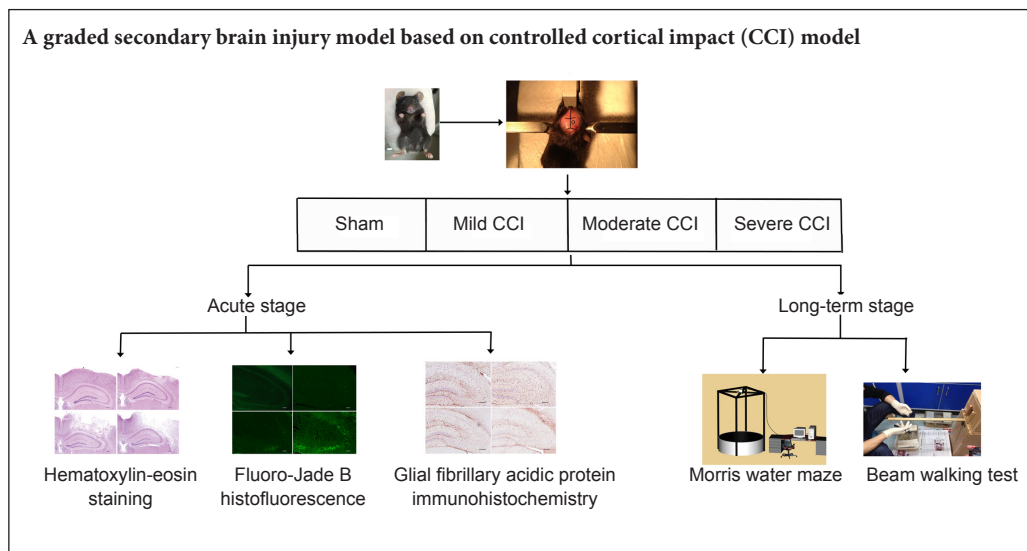
Si-Yi Xu[1, 2, #], Min Liu[2, #], Yang Gao[1], Yang Cao[1], Jin-Gang Bao[1], Ying-Ying Lin[1], Yong Wang[1], Qi-Zhong Luo[1], Ji-Yao Jiang[1], Chun-Long Zhong[2, *]

1 Department of Neurosurgery, Ren Ji Hospital, School of Medicine, Shanghai Jiao Tong University, Shanghai, China
2 Department of Neurosurgery, Shanghai East Hospital, Tongji University School of Medicine, Shanghai, China

Graphical Abstract

A graded secondary brain injury model based on controlled cortical impact (CCI) model

Sham | Mild CCI | Moderate CCI | Severe CCI

Acute stage — Hematoxylin-eosin staining; Fluoro-Jade B histofluorescence; Glial fibrillary acidic protein immunohistochemistry

Long-term stage — Morris water maze; Beam walking test

Correspondence to:
Chun-Long Zhong, MD, PhD,
drchunlongzhong@126.com.

#These authors contributed equally to this work.

orcid:
0000-0002-0605-7273
(Chun-Long Zhong)

Abstract

While animal models of controlled cortical impact often display short-term motor dysfunction after injury, histological examinations do not show severe cortical damage. Thus, this model requires further improvement. Mice were subjected to injury at three severities using a Pin-Point™-controlled cortical impact device to establish secondary brain injury mouse models. Twenty-four hours after injury, hematoxylin-eosin staining, Fluoro-Jade B histofluorescence, and immunohistochemistry were performed for brain slices. Compared to the uninjured side, we observed differences of histopathological findings, neuronal degeneration, and glial cell number in the CA2 and CA3 regions of the hippocampus on the injured side. The Morris water maze task and beam-walking test verified long-term (14–28 days) spatial learning/memory and motor balance. To conclude, the histopathological responses were positively correlated with the degree of damage, as were the long-term behavioral manifestations after controlled cortical impact. All animal procedures were approved by the Institutional Animal Care and Use Committee at Shanghai Jiao Tong University School of Medicine.

Key Words: nerve regeneration; traumatic brain injury; controlled cortical impact; histopathology; behavioral manifestations; neural regeneration

Chinese Library Classification No. R441; R363; R741

Introduction

Traumatic brain injury (TBI) is a common cause of death and disability worldwide, especially in children and young adults. More than 1.7 million people suffer from a TBI in the United States annually (Loane and Faden, 2010). Primary mechanical injury and secondary injury are two major mechanisms of TBI (Loane and Faden, 2010; Marklund and Hillered, 2011). While many studies have focused on secondary damage, the complex relationships between various mediators remain to be verified (Morales et al., 2005; Loane and Faden, 2010; Marklund and Hillered, 2011).

Animal models of TBI are essential for assessing therapeutic interventions (Chen et al., 2017; Xu et al., 2017). The controlled cortical impact (CCI) model is one of the most widely used models of TBI researches (Morales et al., 2005; Albert-Weissenberger and Sirén, 2010; Jiang et al., 2017). The CCI causes a primary brain injury that can imitate a spectrum of contusion injuries, including hippocampal and

thalamic damage (von Baumgarten et al., 2008), extensive cortical tissue loss, cortical spreading depression (Hunt et al., 2009), and post-traumatic epilepsy (Dixon et al., 1991). Because of the utility of genetically engineered mice to study the molecular mechanisms of TBI on post-traumatic outcomes, mouse CCI models are most frequently used.

Previous study has demonstrated that increasing the impact velocity results in increased deficits in motor and cognitive functions in mice; however, cortical damage was not exacerbated (Fox et al., 1998). Increasing the impact depth has been reported to result in an increase in cortical contusion volume but not to exacerbate hippocampal cell loss or motor and cognitive deficits (Rola et al., 2006; Saatman et al., 2006). The dependence of tissue damage on injury severity has not yet been determined in the mouse CCI model, and there is a lack of data on the different morphological and behavioral changes following mild, moderate and severe TBI. Development of a mouse model of graded TBI would be particularly useful in investigating post-traumatic neuron damage and exploring treatment strategies. Thus, this study investigated the acute histopathological responses and long-term behavioral outcomes after graded CCI to provide a comprehensive evaluation of the CCI model in mice.

Materials and Methods
Animals
A total of 152 male C57BL/6 specific-pathogen-free mice weighing 22 ± 4 g and aged 8–12 weeks were obtained from the Shanghai Research Center for Model Organisms, China (license No. SCXK-2014-0002). Mice were housed in groups at 24°C prior to the experiments. To prevent injury from aggression following surgery, the mice were kept in individual cages and allowed free access to food and water. Animals were housed under humidity-controlled (50% relative humidity) conditions with a 12-hour light/dark cycle. All animal procedures were approved by the Institutional Animal Care and Use Committee at Shanghai Jiao Tong University School of Medicine and were performed in accordance with the National Institutes of Health Guide for the Care and Use of Laboratory Animals. Precautions were taken to minimize suffering and the number of animals used in each experiment.

CCI procedure
The mice were randomly assigned to four experimental groups, as follows: sham, mild CCI, moderate CCI, and severe CCI (n = 38 per group). The general health, neurological reflexes, reactivity, and locomotor activity of the CCI groups were not significantly different from those of the sham group.

To induce CCI injury, an intraperitoneal injection of sodium pentobarbital (65 mg/kg) was used to anesthetize the mice, and surgery began once pedal reflexes were absent. The core body temperature was maintained at 37°C on a heating pad and monitored by a rectal thermometer during surgery. The heads of mice were fixed in a stereotaxic frame, and a 4-mm-diameter craniotomy centered at 2.0 mm lat-

eral to the midline over the right hemisphere and 2.0 mm posterior to bregma was performed. The Pin-Point™ CCI device (Model PCI3000, Hatteras Instruments Inc., Cary, NC, USA) had a 3.0-mm rounded metal tip attached to it, which was angled vertically towards the brain surface. A mild injury was induced with a strike velocity of 1.5 m/s and a deformation depth of 1.0 mm; a moderate injury with a strike velocity of 3.0 m/s and a 1.0-mm depth; and a severe injury with 3.0 m/s and a 2.0-mm depth. The duration of the procedure was 180 ms for all groups. After impact, the animal was removed from the stereotaxic holder and the wound was lightly sutured. The sham group underwent the same surgical operations and anesthesia but without CCI injury.

Behavioral assessment
Spatial learning and memory performance was analyzed using the Morris water maze (XR-XM101; Xinruan Information Technology Co., Ltd., Shanghai, China) 11–15 days after injury or sham injury (n = 10 per group) (Morris et al., 1982). The Morris water maze consisted of a large dark pool (120 cm in diameter and 45 cm high) filled with water at a depth of 27 cm and a temperature of 22°C. A Plexiglas platform (8 cm in diameter, 25 cm high) submerged 2 cm below the surface of the water was placed in a fixed position. Each trial began by placing the mice in the water close to and facing the wall of the tank in one of the four start locations. The releasing quadrant was selected randomly and counterbalanced between groups. The mice were allotted 90 seconds to reach the platform, and were allowed to stay on the platform for 30 seconds. When mice did not find the platform, they were placed on it for 30 seconds before the next trial. Before the test trials, mice were pre-trained over three consecutive days (four trials per day). Testing began the day after training had been completed. If the average latency to locate the platform on day 3 was more than 60 seconds, the mice were excluded from the study. In this study, no animal was excluded. The mice performed four trials per day over five consecutive days in the test trials. Behavioral measures were the swim path distance and the mean escape latency. All data were recorded by a computerized analysis system of video motion.

Balance and motor coordination were tested using the beam-walking test (n = 10 per group) (Shear et al., 2004) on days 1, 3, 7, 14, 21, and 28 after injury or sham injury. The apparatus consisted of a narrow wooden beam 120 cm in length, 2 cm in width, and 1.5 cm in height, which was suspended 50 cm above a foam rubber pad. During the testing period, the mice moved to a darkened goal box at the opposite end of the beam, and the running time was recorded (up to 60 seconds maximum). The mice were trained over two days before injury or sham injury. The mice were trained until they could pass the beam in less than 15 seconds.

Tissue sectioning and collection
In each of the four groups, 18 animals were used for hematoxylin-eosin staining, Fluoro-Jade B (FJB) staining, and

glial fibrillary acidic protein (GFAP) staining. The mice were euthanized 24 hours after CCI by intraperitoneally injecting sodium pentobarbital 65 mg/kg, and perfused transcardially with phosphate buffered saline followed by 50 mL of 4% paraformaldehyde. The brains were removed quickly and fixed in 4% paraformaldehyde at 4°C for about 48 hours. Coronal sections, which contained the entire hippocampus (–0 mm, –3.5 mm relative to bregma), were obtained using a vibratome (Leica VT 1000S, Wetzlar, Germany). Serial coronal sections (30-μm thick) were cut by a cryostat (Leica CM 1950) for hematoxylin-eosin staining ($n = 6$ per group). For FJB histofluorescence ($n = 6$ per group), frozen brain sections (−20°C) at a thickness of 30 μm were obtained and saved in 24-well cell culture plates. Every eighth section was sampled, and a total of 10 sections per brain was collected and analyzed. For GFAP immunohistochemistry ($n = 6$ per group), the brain tissues containing the entire hippocampus were embedded in paraffin and sliced into 6-μm thick coronal sections at 200-μm intervals. Twelve sections in each brain were collected and analyzed.

Hematoxylin-eosin staining
Brain sections were rinsed with dH$_2$O and stained in hematoxylin for 6 minutes, and were then decolorized in acid alcohol for 1 second. Before being immersed in LiCO$_3$, the sections were rinsed with dH$_2$O for 3 seconds and were counterstained in eosin for 15 seconds. Afterwards, the sections were rinsed with dH$_2$O and dehydrated with 95% ethyl alcohol for 2–3 minutes and 100% ethyl alcohol for 2–3 minutes. The sections were then cleared with xylene for 2–5 minutes, mounted with DePeX (Thermo Fisher Scientific Inc., Waltham, MA, USA) in a fume hood, and visualized using an inverted microscope at 100× magnification (Nikon, Tokyo, Japan). Digital images were captured with a SPOT microscope camera (Diagnostic Instruments, Sterling Heights, MI, USA).

FJB histofluorescence
To identify degenerating neurons, FJB histofluorescence was performed. The mounted tissue sections were submersed in 100% ethyl alcohol for 3 minutes, followed by 70% ethyl alcohol for 1 minute, dH$_2$O for 1 minute, and 0.006% potassium permanganate for 15 minutes. After being rinsed in dH$_2$O for 1 minute, the sections were incubated in 0.001% FJB (Cell Signaling Technology, Beverly, MA, USA) staining solution in 0.1% acetic acid for 30 minutes. Afterwards, the sections were submersed in xylene and cover slipped with DePeX mounting medium (CTM6; Thermo Fisher Scientific Inc.). FJB-stained sections were captured under ultraviolet light by a fluorescent microscope (90i; Nikon) equipped with digital cameras and a fluorescein isothiocyanate filter.

Immunohistochemistry
GFAP immunolocalization was performed to label astrocytes (Kunkler and Kraig, 1997). The tissue sections were deparaffinized twice (15 minutes each) into xylene, and then four times (5 minutes each) in graded ethyl alcohols. After

two washes with phosphate buffered saline, the sections were placed into an antigen retrieval buffer and heated in a microwave at a medium power for 15–20 minutes. To block endogenous peroxidase activity, after being rinsed with phosphate buffered saline, the sections were incubated in 3% H$_2$O$_2$ solution for 10 minutes. The sections were rinsed three times (3 minutes each) in phosphate buffered saline and incubated in a blocking solution (5% goat serum in phosphate buffered saline) for 1 hour at 20°C. The sections were incubated overnight with primary anti-GFAP antibody (rabbit anti-mouse, 1:1000; Chemicon AB-5804, Temecula, CA, USA) at 4°C. After three washes with phosphate buffered saline, the sections were incubated with biotinylated secondary antibody (goat anti-rabbit, 1:500; Vector Labs BA-1000, Burlingame, CA, USA) for 2 hours at 20°C. Finally, immunodetection was achieved using the Vectastain Elite ABC amplification kit (Vector Labs), followed by color development with chromogen. After a series of dehydration steps using xylene and ethyl alcohol, the sections were mounted onto slides. The sections were visualized under an inverted microscope at 100× magnification (Nikon) and digital images were captured with a SPOT microscope camera (Diagnostic Instruments).

Quantification of histopathology
The "scan" function (Nikon 90i) was used to obtain multiple partial images of images to the hippocampal CA2/3 regions. Then, partial images were joined into a complete image and were digitally reconstructed into a montage (ImageJ, National Institutes of Health, Bethesda, MD, USA). The number of marked cells in the hippocampal CA2/3 regions in each photo was quantified, and their ratio to the hippocampal CA2/3 regions in each of the photo was calculated using a density function. The mean densities of positive cells were determined for every hippocampal section. The photographs were analyzed by observers that were blinded to the study conditions.

Statistical analysis
All data were analyzed using SPSS 19.0 software (IBM SPSS Inc., Chicago, IL, USA), and are expressed as the mean ± SEM. Two-tailed Student's *t*-tests assuming unequal variances were used to analyze the latency to reach the hidden platform of experiment animals. Density of astrocytes and degenerating neurons was analyzed using a one-way analysis of variance with Bonferroni *post hoc* tests. The latencies to find a hidden platform in Morris water maze test and the latencies to cross the beam in beam walk test were analyzed using a repeated measures analysis of variance (group × days) followed by Bonferroni tests for group comparisons. The significance level was set to $P < 0.05$.

Results
Acute histopathological responses after graded cortical impact injury in mice
Hematoxylin-eosin staining revealed a progressive loss of cortical tissue and distortions in the morphology of the re-

maining cortex 24 hours after CCI (**Figure 1**). In the mild CCI group, there was slight brain tissue loss compared with the sham group (**Figure 1B**). In the moderate CCI group, there was obvious cortical tissue loss compared with the sham and mild CCI groups (**Figure 1C**). In the severe CCI group, the cortical tissue loss was most significant among all groups (**Figure 1D**).

FJB staining revealed there was no evidence of degenerating neurons in the ipsilateral hippocampus of the sham group (**Figure 2A**). However, 24 hours after CCI, FJB-positive neurons were observed in the stratum pyramidale. In the moderate and severe CCI groups (**Figure 2C** and **D**), brightly fluorescent pyramidal cells with extensive dendritic arborization into the stratum radiatum were found in the CA2/3 regions. In the mild CCI group (**Figure 2B**), FJB-positive neurons were also visible in the CA2/3 regions of the hippocampus. Moderate and severe CCI groups exhibited a significantly increased number of degenerating neurons than the mild group in the CA2/3 regions after CCI compared with the mild CCI group ($P < 0.01$; **Figure 2E**). No distinct FJB-positive neurons were observed in the region of interest of the contralateral hemisphere of all four groups.

In the sham group, the GFAP-positive astrocytes identified in the ipsilateral hemisphere CA2/3 regions appeared "normal" (with a distinct cell soma and clearly identifiable foot processes) (**Figure 3A**). In the CCI groups, GFAP staining revealed a significant decrease in number of the ipsilateral astrocytes compared with the sham group in the CA2/3 regions, and some astrocytes had a fragmented appearance that is characteristic of necrotic cells. At 24 hours after CCI, fewer GFAP-positive cells in the target region were identified in the mild CCI group (**Figure 3B**) compared with the moderate and severe CCI groups (**Figure 3C–E**).

Long-term behavioral outcomes after graded cortical impact injury in mice

Moderate and severe CCI groups showed impaired Morris water maze task behaviors compared with the sham group (**Figure 4A**). There were significant differences in latency to find a hidden platform in Morris water maze test in all CCI groups (all $P < 0.01$) compared with the sham group. On testing days, the latency to find the hidden platform was significantly longer in the CCI groups than in the sham group (all $P < 0.01$). The latency to find the platform in the moderate CCI group was significantly shorter than that of the severe CCI group on days 13, 14, and 15 after injury ($P < 0.01$). There were no significant between-group differences in swim speeds (sham group: 18.9 ± 3.3 cm/s; mild CCI group: 19.6 ± 3.5 cm/s; moderate CCI group: 18.3 ± 4.2 cm/s; severe CCI group: 17.9 ± 2.6 cm/s).

The beam-walking task performance was also impaired in the CCI groups (**Figure 4B**). On testing days, *post hoc* Bonferroni tests showed that the CCI groups had significantly longer beam walking latencies than the sham group ($P < 0.01$). However, the moderate CCI group showed a significantly shorter beam walking latency than the severe CCI group ($P < 0.01$) on days 14, 21, and 28 after CCI.

Discussion

In this study, we identified suitable impact parameters for the CCI device and assessed the acute histopathological responses and long-term behavioral outcomes after graded CCI in mice. Mice were subjected to CCI at three severities by a Pin-Point™ CCI device and sacrificed 24 hours later. Subsequently, their brains were processed according to the hematoxylin-eosin staining, FJB histofluorescence, and GFAP immunohistochemistry protocols. In addition, CCI-induced deficits in long-term spatial learning/memory and motor balance control abilities were evaluated using the Morris water maze and the beam-walking test, respectively. Histological analysis demonstrated a clear gradation of subcortical tissue damage, neuronal degeneration, and astrocyte loss in the CA2/3 regions of the hippocampus 24 hours after the graded CCI injuries. Moreover, CCI produced long-term behavioral deficits in a severity-dependent manner.

The CCI device used in our study reported that it allows variable parameters of the tip motion to produce injuries (Bilgen, 2005). However, there is a lack of data on the graded morphological and behavioral changes in the acute stage and long-term outcomes during the postoperative course in CCI models. Therefore, this study investigated the acute histopathological responses and long-term behavioral outcomes after graded CCI in mice to supplement the development of the CCI model in mice.

The present study evaluated the acute histological outcome in the CA2/3 regions of the hippocampus 24 hours after CCI. In CCI model, the hippocampus undergoes similar neuropathological changes (Saatman et al., 2006) to another two TBI models, fluid percussion (Thompson et al., 2005) and stretch injury (McCarthy, 2003). Hippocampal volume was used as an parameter to evaluate the severity of TBI, which also suggests that the hippocampus is particularly vulnerable to secondary injury following TBI (Isoniemi et al., 2006). Despite the unique features of each model in previously mentioned studies, the temporal and regional patterns of subcortical neuronal loss are similar to those after TBI. This is perhaps best exemplified in the predictable pattern of neuronal cell loss in the hippocampus and thalamus (Chen et al., 2003), which probably contributes to functional deficits, including cognitive impairment (Smith et al., 1995). Thus, craniotomies were performed after the examination (cortical tissue loss was observed by hematoxylin-eosin staining, and hippocampal CA2/3 region cell loss/survival was observed by FJB and GFAP staining).

Injured neurons were identified using FJB, a fluorescent marker of neuronal degeneration (Freyaldenhoven et al., 1997; Schmued et al., 1997). In this study, FJB was indeed found to be a relatively simple technique for staining the entirety of injured neurons, including cell bodies, dendrites, axons, and terminals. FJB-stained neurons were present in the mild CCI group, but the number of stained neurons was greater in the moderate and severe CCI groups.

Some studies have examined astrocytic activation after TBI, which is characterized by enhanced expression of glial scarring and GFAP (Kunkler and Kraig, 1997; Wang et al.,
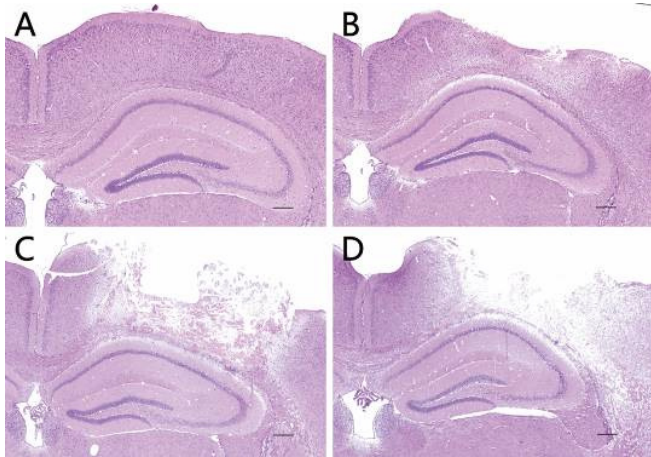
Figure 1 Histological characteristics of the injured brain 24 hours after controlled cortical impact.

(A–D) Histological images of hematoxylin-eosin-stained coronal sections showing the brain architecture and tissue loss 24 hours post CCI. Brain tissue injury and anatomical distortion increase in a graded fashion with increased impact parameters. (A) Sham group; (B) mild CCI group: slight tissue deformation; (C) moderate CCI group: obvious loss of cortical tissue at the impact site; (D) severe CCI group: a significant cortical tissue loss (n = 6 mice per group). Scale bars: 200 μm.
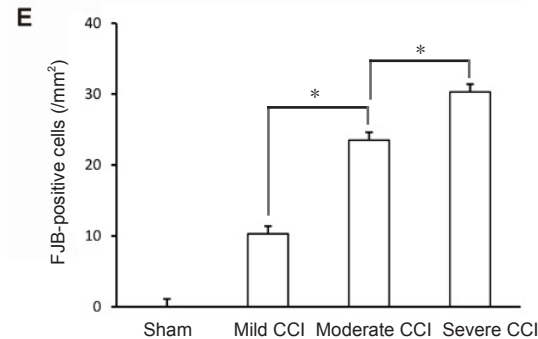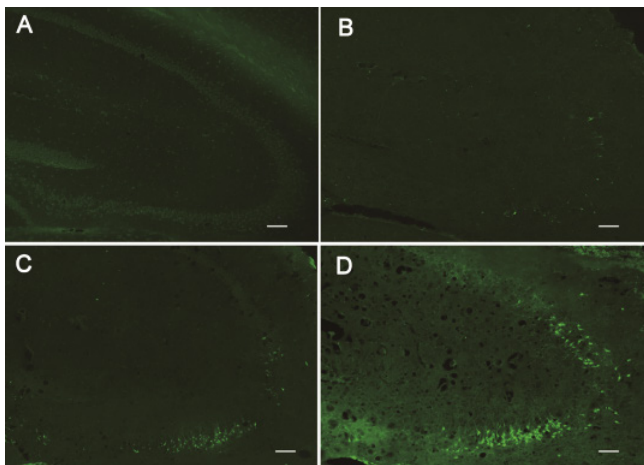
Figure 2 FJB histofluorescence of degenerating neurons in the ipsilateral CA2/3 regions in mice 24 hours after CCI.

(A) FJB histofluorescence (green) of degenerating neurons in sham, mild CCI, moderate CCI, and severe CCI groups. Scale bars: 100 μm. (E) Amount of degenerating neurons stained by FJB. Data are expressed as the mean ± SEM (n = 6 per group; one-way analysis of variance followed by *post hoc* Bonferroni *t*-tests). *P < 0.01. FJB: Fluoro-Jade B; CCI: controlled cortical impact.
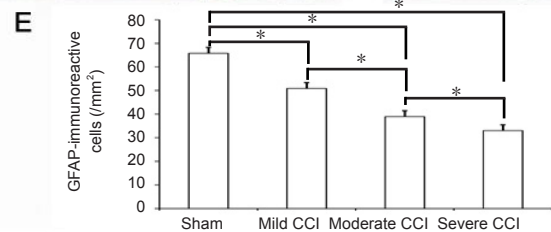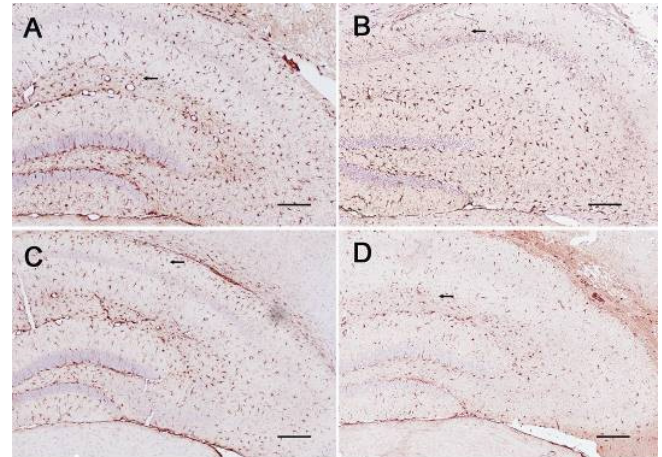
Figure 3 GFAP immunoreactivity of astrocytes in the ipsilateral CA2/3 regions 24 hours after CCI.

(A) GFAP immunoreactivity (arrows) in the sham, mild CCI, moderate CCI, and severe CCI groups. Scale bars: 100 μm. (E) Quantification of GFAP-immunoreactive astrocytes in the ipsilateral hemisphere. Data are expressed as the mean ± SEM (n = 6 per group; one-way analysis of variance followed by *post hoc* Bonferroni *t*-tests). *P < 0.01. GFAP: Glial fibrillary acidic protein; CCI: controlled cortical impact.
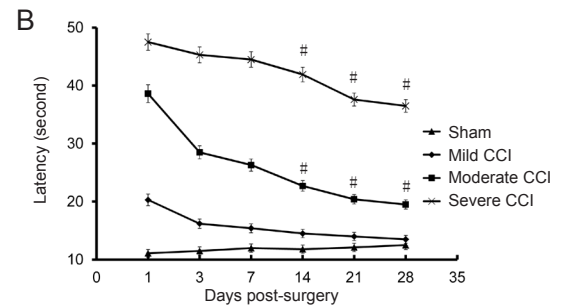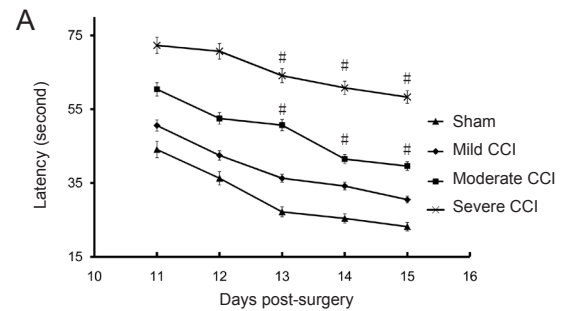
Figure 4 Effect of CCI on motor behavior in mice.

(A) Assessment of the Morris water maze test after CCI: The latencies to find a hidden platform were significantly longer in the moderate and severe CCI groups than in the sham group, on all test days (#P < 0.01). (B) Assessment of beam walking after CCI: The latencies to cross the beam were significantly longer in the moderate and severe CCI groups compared with the sham group, on all test days (#P < 0.01). Data are expressed as the mean ± SEM (n = 10 per group; repeated measures analysis of variance (group × days) followed by Bonferroni *t*-tests). #P < 0.01, *vs.* sham group. CCI: Controlled cortical impact.

2018). However, one study reported no changes in the proliferation of astrocytes in the cortex surrounding the trauma site (Dvela-Levitt et al., 2014). Ekmark-Lewén et al. (2010) and Huang et al. (2015) reported that there was an elevation of GFAP in hippocampus, cerebrospinal fluid and serum after TBI. Previous studies have demonstrated that reactive astrocytes are typically observed at later time points after experimental TBI (Dunn-Meynell and Levin, 1997; Hellewell et al., 2010). Meanwhile, other studies have reported a decrease in the number of astrocytes in the hippocampus, an area that is commonly susceptible to excitotoxicity, following moderate TBI (Zhao et al., 2003; Zhong et al., 2005; Gao et al., 2015; Cao et al., 2016), which is consistent with our results. Furthermore, astrocytes may be damaged following central nervous system injury prior to the development of reactive gliosis (Liu et al., 1999). The results of the present investigation support the conclusion that astrocytes may be rapidly damaged in selectively vulnerable brain regions following acute CCI. We found that the number of GFAP-positive cells was reduced in the CA2/3 region of the hippocampus with the increase in CCI severity. The different results of GFAP immunohistochemistry might due to a variety of species, region, model, or time.

Neurofunctional outcome tests during the recovery phase was suggested to be important to evaluate the levels of CCI and behavioral deficits (Scheff et al., 2003). All the CCI groups had a significantly longer latency to find the platform in the Morris water maze than the sham group on day 11. This indicates that CCI resulted in a reduced ability to find and/or learn the location of the platform. From days 11 to 15, the ability of the mild CCI group to learn/recall the location of the platform was comparable to the sham group, while the moderate and severe CCI groups showed no such improvements over this time interval. These results demonstrate that CCI induced impairments in learning and/or retrieval. As TBI leads to multiple short- and long-term changes in neuronal circuits (Guerriero et al., 2015). To investigate whether the cognitive impairment exhibited in the Morris water maze task was a transient effect of CCI, the time interval was extended to 28 days to assess the long-term effects of CCI. Motor function was evaluated at postoperative days 1–28 using the beam-walking task. The beam-walking test also presented obvious differences similar to what we found in Morris water maze task.

In summary, the graded CCI injuries produced a clear gradation of acute and long-term brain damage, which suggests that the current CCI mouse model offers sensitive, reliable evidence for assessments of therapeutic strategies for TBI.

References

Albert-Weissenberger C, Sirén AL (2010) Experimental traumatic brain injury. Exp Transl Stroke Med 2:16.

Bilgen M (2005) A new device for experimental modeling of central nervous system injuries. Neurorehabil Neural Repair 19:219-226.

Cao Y, Gao Y, Xu S, Bao J, Lin Y, Luo X, Wang Y, Luo Q, Jiang J, Neale JH, Zhong C (2016) Glutamate carboxypeptidase II gene knockout attenuates oxidative stress and cortical apoptosis after traumatic brain injury. BMC Neurosci 17:15.

Chen S, Pickard JD, Harris NG (2003) Time course of cellular pathology after controlled cortical impact injury. Exp Neurol 182:87-102.

Chen T, Yu Y, Tang LJ, Kong L, Zhang CH, Chu HY, Yin LW, Ma HY (2017) Neural stem cells over-expressing brain-derived neurotrophic factor promote neuronal survival and cytoskeletal protein expression in traumatic brain injury sites. Neural Regen Res 12:433-439.

Dixon CE, Clifton GL, Lighthall JW, Yaghmai AA, Hayes RL (1991) A controlled cortical impact model of traumatic brain injury in the rat. J Neurosci Methods 39:253-262.

Dunn-Meynell AA, Levin BE (1997) Histological markers of neuronal, axonal and astrocytic changes after lateral rigid impact traumatic brain injury. Brain Res 761:25-41.

Dvela-Levitt M, Ami HC-B, Rosen H, Shohami E, Lichtstein D (2014) Ouabain improves functional recovery following traumatic brain injury. J Neurotrauma 31:1942-1947.

Ekmark-Lewén S, Lewén A, Israelsson C, Li GL, Farooque M, Olsson Y, Ebendal T, Hillered L (2010) Vimentin and GFAP responses in astrocytes after contusion trauma to the murine brain. Restor Neurol Neurosci 28:311-321.

Fox GB, Fan L, Levasseur RA, Faden AI (1998) Sustained sensory/motor and cognitive deficits with neuronal apoptosis following controlled cortical impact brain injury in the mouse. J Neurotrauma 15:599-614.

Freyaldenhoven TE, Ali SF, Schmued LC (1997) Systemic administration of MPTP induces thalamic neuronal degeneration in mice. Brain Res 759:9-17.

Gao Y, Xu S, Cui Z, Zhang M, Lin Y, Cai L, Wang Z, Luo X, Zheng Y, Wang Y, Luo Q, Jiang J, Neale JH, Zhong C (2015) Mice lacking glutamate carboxypeptidase II develop normally, but are less susceptible to traumatic brain injury. J Neurochem 134:340-353.

Guerriero RM, Giza CC, Rotenberg A (2015) Glutamate and GABA imbalance following traumatic brain injury. Curr Neurol Neurosci Rep 15:27.

Hellewell SC, Yan EB, Agyapomaa DA, Bye N, Morganti-Kossmann MC (2010) Post-traumatic hypoxia exacerbates brain tissue damage: analysis of axonal injury and glial responses. J Neurotrauma 27:1997-2010.

Huang XJ, Glushakova O, Mondello S, Van K, Hayes RL, Lyeth BG (2015) Acute temporal profiles of serum levels of UCH-L1 and GFAP and relationships to neuronal and astroglial pathology following traumatic brain injury in rats. J Neurotrauma 32:1179-1189.

Hunt RF, Scheff SW, Smith BN (2009) Posttraumatic epilepsy after controlled cortical impact injury in mice. Exp Neurol 215:243-252.

Isoniemi H, Kurki T, Tenovuo O, Kairisto V, Portin R (2006) Hippocampal volume, brain atrophy, and APOE genotype after traumatic brain injury. Neurology 67:756-760.

Jiang L, Hu Y, He X, Lv Q, Wang TH, Xia QJ (2017) Breviscapine reduces neuronal injury caused by traumatic brain injury insult: partly associated with suppression of interleukin-6 expression. Neural Regen Res 12:90-95.

Kunkler PE, Kraig RP (1997) Reactive astrocytosis from excitotoxic injury in hippocampal organ culture parallels that seen in vivo. J Cereb Blood Flow Metab 17:26-43.

Liu D, Smith CL, Barone FC, Ellison JA, Lysko PG, Li K, Simpson IA (1999) Astrocytic demise precedes delayed neuronal death in focal ischemic rat brain. Brain Res Mol Brain Res 68:29-41.

Loane DJ, Faden AI (2010) Neuroprotection for traumatic brain injury: translational challenges and emerging therapeutic strategies. Trends Pharmacol Sci 31:596-604.

Marklund N, Hillered L (2011) Animal modelling of traumatic brain injury in preclinical drug development: where do we go from here? Br J Pharmacol 164:1207-1229.

McCarthy MM (2003) Stretching the truth: Why hippocampal neurons are so vulnerable following traumatic brain injury. Exp Neurol 184:40-43.

Morales DM, Marklund N, Lebold D, Thompson HJ, Pitkanen A, Maxwell WL, Longhi L, Laurer H, Maegele M, Neugebauer E, Graham DI, Stocchetti N, McIntosh TK (2005) Experimental models of traumatic brain injury: Do we really need to build a better mousetrap? Neuroscience 136:971-989.

Morris RG, G0arrud P, Rawlins JN, O'Keefe J (1982) Place navigation impaired in rats with hippocampal lesions. Nature 297:681-683.

Rola R, Mizumatsu S, Otsuka S, Morhardt DR, Noble-Haeusslein LJ, Fishman K, Potts MB, Fike JR (2006) Alterations in hippocampal neurogenesis following traumatic brain injury in mice. Exp Neurol 202:189-199.

Saatman KE, Feeko KJ, Pape RL, Raghupathi R (2006) Differential behavioral and histopathological responses to graded cortical impact injury in mice. J Neurotrauma 23:1241-1253.

Scheff SW, Rabchevsky AG, Fugaccia I, Main JA, Lumpp JE (2003) Experimental modeling of spinal cord injury: characterization of a force-defined injury device. J Neurotrauma 20:179-193.

Schmued LC, Albertson C, Slikker W Jr (1997) Fluoro-Jade: a novel fluorochrome for the sensitive and reliable histochemical localization of neuronal degeneration. Brain Res 751:37-46.

Shear DA, Tate MC, Archer DR, Hoffman SW, Hulce VD, LaPlaca MC, Stein DG (2004) Neural progenitor cell transplants promote long-term functional recovery after traumatic brain injury. Brain Res 1026:11-22.

Smith DH, Soares HD, Pierce JS, Perlman KG, Saatman KE, Meaney DF, Dixon CE, McIntosh TK (1995) A model of parasagittal controlled cortical impact in the mouse: cognitive and histopathologic effects. J Neurotrauma 12:169-178.

Thompson HJ, Lifshitz J, Marklund N, Grady MS, Graham DI, Hovda DA, McIntosh TK (2005) Lateral fluid percussion brain injury: a 15-year review and evaluation. J Neurotrauma 22:42-75.

von Baumgarten L, Trabold R, Thal S, Back T, Plesnila N (2008) Role of cortical spreading depressions for secondary brain damage after traumatic brain injury in mice. J Cereb Blood Flow Metab 28:1353-1360.

Wang D, Xu X, Wu YG, Lyu L, Zhou ZW, Zhang JN (2018) Dexmedetomidine attenuates traumatic brain injury: action pathway and mechanisms. Neural Regen Res 13:819-826.

Xu HH, Dong HJ, Shang CZ, Zhao ML (2017) Umbilical cord mesenchymal stem cell transplantation increases microvessel density in surrounding areas of acute traumatic brain injury in rats. Zhongguo Zuzhi Gongcheng Yanjiu 21:5320-5324.

Zhao X, Ahram A, Berman RF, Muizelaar JP, Lyeth BG (2003) Early loss of astrocytes after experimental traumatic brain injury. Glia 44:140-152.

Zhong C, Zhao X, Sarva J, Kozikowski A, Neale JH, Lyeth BG (2005) NAAG peptidase inhibitor reduces acute neuronal degeneration and astrocyte damage following lateral fluid percussion TBI in rats. J Neurotrauma 22:266-276.